Article
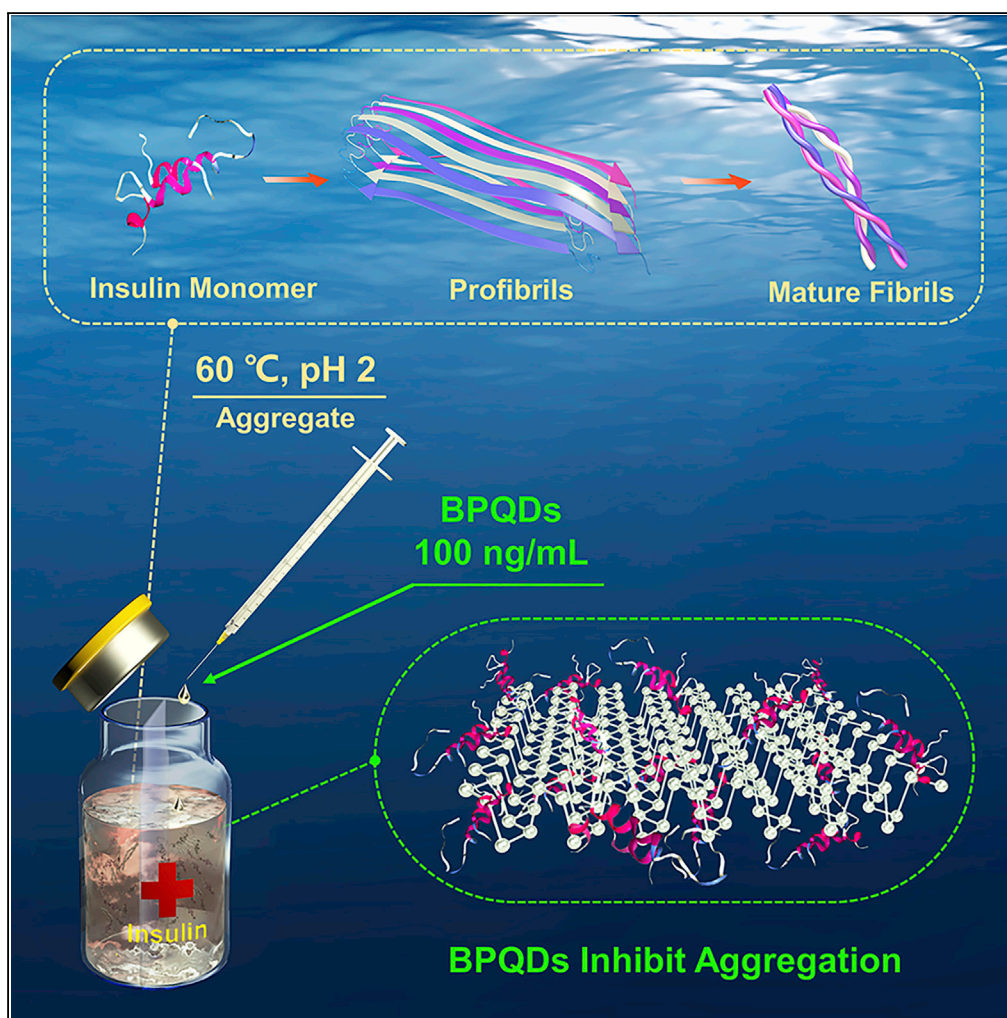
Nontoxic Black Phosphorus Quantum Dots Inhibit Insulin Amyloid Fibrillation at an Ultralow Concentration

Siqi Wang,
Chuanxi Li,
Yinqiang Xia, ...,
Wei Qi, Zhimin He,
Rongxin Su

surx@tju.edu.cn

HIGHLIGHTS

BPQDs inhibit insulin amyloid fibrillation at an ultralow concentration

BPQDs can depolymerize protofibrils and even mature fibers

BPQDs inhibit aggregation mainly by van der Waals' force and hydrophobic interaction

BPQDs are biocompatible and can reduce insulin fibrils-induced cytotoxicity

Article

Nontoxic Black Phosphorus Quantum Dots Inhibit Insulin Amyloid Fibrillation at an Ultralow Concentration

Siqi Wang,[1,6] Chuanxi Li,[1,6] Yinqiang Xia,[1] Shaohuang Chen,[1] Jordan Robert,[2] Xavier Banquy,[2] Renliang Huang,[3] Wei Qi,[1,4] Zhimin He,[1] and Rongxin Su[1,4,5,7,*]

SUMMARY

Amyloid are protein aggregates formed by cross β structures assemblies. Inhibiting amyloid aggregation or facilitating its disassembly are considered to be two major effective therapeutic strategies in diseases involving peptide or protein fibrillation such Alzheimer's disease or diabetes. Using thioflavin-T fluorescence, far-UV circular dichroism spectroscopy, and atomic force microscopy, we found nontoxic and biocompatible black phosphorus quantum dots (BPQDs) appear to have an exceptional capacity to inhibit insulin aggregation and to disassemble formed mature fibrils, even at an ultralow concentration (100 ng/mL). The inhibition of fibrillation persists at all stages of insulin aggregation and increases PC12 cells survival when exposed to amyloid fibrils. Molecular dynamics simulations suggest that BPQDs are able to stabilize the α-helix structure of insulin and obliterate the β-sheet structure to promote the fibril formation. These characteristics make BPQDs be promising candidate in preventing amyloidosis, disease treatment, as well as in the storage and processing of insulin.

INTRODUCTION

Amyloid fibrils containing highly ordered β-sheet structure have been found to be one of the most prominent pathological features of a variety of diseases, including Alzheimer's disease, Parkinson's disease, Huntington's disease, prion conditions, and type II diabetes (Goedert and Spillantini, 2006; Shulman et al., 2011; Walker, 2007; Eisenberg and Jucker, 2012; Chiti and Dobson, 2006). Numerous studies have demonstrated that insoluble amyloid fibrils possess significant cytotoxicity (Pike et al., 1993; Petkova et al., 2005) and new drugs such as amyloid inhibitors could be promising therapeutic avenue.

Therapeutic strategies directed at targeting amyloidosis are divided into two main categories: the inhibition of fibrils formation or the elimination of amyloid fibrils. Depending on the strategy used, different types of inhibitors have been discovered and studied over the past decade. An emerging example of such inhibitors are nanomaterials that have demonstrated remarkable ability to interact strongly with amyloids and amyloid fibrils owing to their large surface area, unique physical properties, and small size (Yousaf et al., 2017; Wang et al., 2017). On the one hand, some nanoparticles, such as titanium dioxide nanoparticles (Wu et al., 2008), carbon nanotubes, and cerium oxide nanoparticles (Linse et al., 2007), have been reported to promote the nucleation step of amyloid fibrillation and exacerbate amyloid-related diseases. On the other hand, a number of studies have proven that nanomaterials such as carbon dots (Li et al., 2015), graphene oxide (Li et al., 2012; Wang et al., 2019), N-acetyl-L-cysteine-capped CdTe quantum dots (Xiao et al., 2010), thioglycolic acid-capped CdTe quantum dots (Yoo et al., 2011), and dihydrolipoic acid-capped CdSe/ZnS quantum dots (Thakur et al., 2011) can efficiently delay nucleation or inhibit fibrils formation. These nanomaterials have attracted a lot of attention due to their outstanding inhibitory effect (Wang et al., 2017; Cabaleiro-Lago et al., 2010). Several strategies have been suggested to further enhance nanomaterials capacity to inhibit fibrillation. For example, Xiong et al. (2017) have conjugated two peptide inhibitors (VVIA and LPFFD) onto gold nanoparticles (AuNPs) and demonstrated that the inhibition activity of the corresponding peptide@AuNPs was 50% enhanced compared with peptides alone. Nanomaterials can not only inhibit fibrillation but can also effectively destroy and clear pre-formed fibrillary structures. Recently, Kim et al. (2018) found that graphene quantum dots induced the dissociation of α-synuclein fibrils into short fragments. Yin et al. (2016) used penetratin peptide-loaded PEG-stabilized gold nanostars modified with ruthenium complex to remotely dissociate preformed fibrous Aβ fibrils under near-infrared irradiation.

Nevertheless, the toxicity of nanomaterials should not be ignored in *in vivo* applications. Reactive oxygen species (ROS) generation is one of the important mechanisms of nanoparticle-induced toxicity. ROS can trigger the generation of oxidative stress and even damage mitochondria, which in turn triggers a series of mitochondrial-mediated toxic effects (Wu et al., 2020; Yang et al., 2019). For example, CdTe quantum dots can not only damage mitochondria, but also exert endothelial toxicity by activating mitochondrial death pathways and inducing endothelial cell apoptosis (Yan et al., 2011). Metal ions may be released after partial biodegradation of metal nanomaterials, resulting in potential metal dyshomeostasis associated with side effects (Yang et al., 2019). In addition, the contamination of residual impurities in nanomaterials is also considered as a major risk factor. For example, nickel, yttrium, or rubidium metal impurities may be present on the surface of carbon nanotubes (Jeevanandam et al., 2018). The omnipresent toxic effect of most nano-materials limits the therapeutic window of these materials, which lowers significantly their ability to inhibit amyloid fibrillation. Therefore, highly efficient, non-toxic, and biodegradable amyloid targeted inhibitors are still highly demanded for both defibrillation and inhibition of amyloid proteins fibrillation.

Black phosphorus quantum dot (BPQD) is a novel kind of zero-dimensional layered nanomaterial that has drawn increasing attention in recent years. Owing to the lone pair of electrons on the outer orbitals of the phosphorus atom, BPQDs are easily oxidized into non-toxic phosphate (Luo et al., 2019). OH^- initiated the decomposition of BP through breaking the P-P bond and forming a P-O bond, and the degradation process of BP could be regulated by changing the pH (Zhang et al., 2019). The chemical instability of BPQDs contributes to their biocompatibility and biodegradation (Zhang et al., 2018) and has proven to benefit their biomedical application in tumor photothermal therapy, drug delivery, and therapeutic diagnostics (Luo et al., 2019; Choi et al., 2018). Pathological evaluation of tissues obtained from the lung, liver, spleen, kidney, and heart of BPQDs-treated mice at 1, 10, and 30 days post injection demonstrate that the BPQDs have good biocompatibility for these organs of the mice during the entire period (Wang et al., 2018a). Additionally, BP nanosheets have been reported to effectively capture excess Cu^{2+} and to form non-toxic metal complex, therefore protecting neuronal cells from ROS toxicity caused by Cu^{2+}, a key benefit for the treatment of neurodegenerative diseases (Chen et al., 2018). Some modified BP can inhibit Aβ aggregation. For instance, the photo-excited BP@BTA (BTA: one of thioflavin-T derivatives) can generate singlet oxygen ($^1O_2$) to oxygenate Aβ under NIR laser, which inhibits the aggregation and reduces the Aβ-induced cytotoxicity (Li et al., 2019). Lim et al. (2019) found that, when the mass ratio of Aβ40 to BP is greater than 1:0.25, the titanium ligand-modified BP nanosheets can reduce total amounts of aggregated Aβ40, but they cannot delay the initiation of Aβ40 aggregation. Therefore, BP has great application potential in the field of regulating amyloid fibrosis. However, the effect of BPQDs on peptide or protein fibrils inhibition has not been clearly delineated yet.

To further investigate the interaction between BPQDs and amyloid fibrils, insulin, an important therapeutic protein for type II diabetes condition, was chosen as a model protein (Scheme 1). The amyloidogenesis of insulin reduces the efficacy of insulin administrations and disturbs insulin delivery, which may lead to diabetic ketoacidosis, a life-threatening complication. Besides, insulin amyloid fibrillation is one of the major issues in the processes of its production, storage, and delivery (Li et al., 2015; Ratha et al., 2016). In the present study, amyloid fibrosis was monitored by thioflavin-T (ThT) fluorescence, far-UV circular dichroism (CD) spectroscopy, and atomic force microscopy (AFM). Addition of BPQDs significantly inhibited the conversion of insulin into amyloid fibrils over several days at extremely low concentrations never attained by any other nanomaterial reported so far. Molecular dynamics (MD) simulation was used to provide further insights into this remarkable effect. In addition, the cytotoxicity of BPQDs and insulin solutions exposed to different concentrations of BPQDs was evaluated using *in vitro* cell toxicity assays. Overall, results show that an ultralow concentration of BPQDs acts as potent and non-toxic amyloid fiber inhibitor, which offers great potential in the development of diabetes treatment and other diseases involving amyloid fibrillation.

RESULTS

Inhibition of Insulin Aggregation and Fibrillation by BPQDs

BPQDs were prepared via a liquid exfoliation method as reported before in our laboratory, and the average lateral size of BPQDs is about 3 nm (Xia et al., 2018). Accelerated insulin aggregation was triggered by heat treatment (60°C, 48 h at pH = 2) to denature α-helix structures in the protein and promote β-sheets refolding, a necessary step to aggregation and fibrillation. Different concentrations of BPQDs (0, 50, 100, 200, 500 ng/mL) were co-incubated with denatured insulin to study the inhibitory effect of BPQDs on amyloid
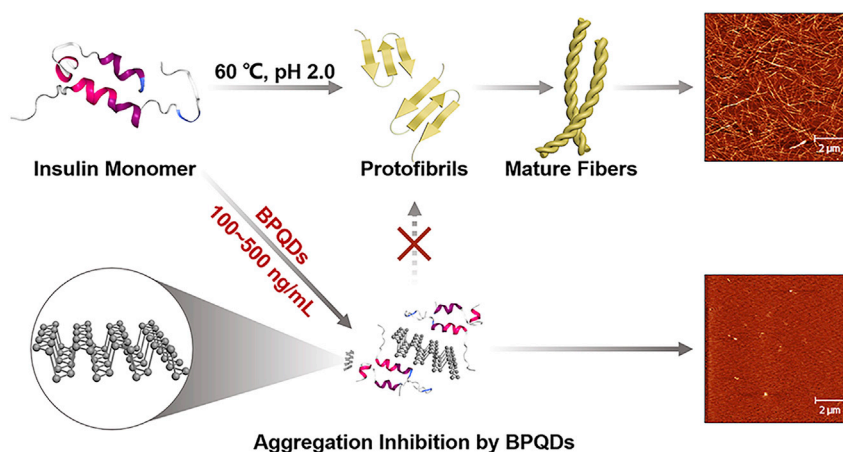
Scheme 1. Schematic Representation of Amyloid Aggregation of Insulin in the Absence and Presence of BPQDs

The insulin monomers were all incubated at 60°C and pH 2.0. Stable amyloid fibrils made of pure insulin were formed after 2 days, whereas no significant fibrils were observed after 7 days in the presence of BPQDs. The illustrations are AFM images of insulin amyloid aggregation after 7 days.

fibrillation. The aggregation kinetics of amyloid was monitored by ThT fluorescence assay. ThT is an extrinsic fluorescent dye that can specifically bind to the β-sheet structure of amyloid fibrils, and its fluorescence intensity increases with the content of β-sheet structure (Liu et al., 2015; Niu et al., 2016; Biancalana and Koide, 2010).

As shown in Figure 1A, the aggregation kinetics (black line) of insulin alone presented three stages characteristic of a typical nucleation-dependent fibrillation process: first, a lag phase were no apparent aggregation is observed, followed by the elongation phase were aggregation and fibrillation occur simultaneously, and finally a saturation phase were mature fibrils are fully formed and monomeric insulin is derived from the medium (Lee et al., 2007, 2011). The lag phase was observed to be as long as 12 h in the measurement and concentration conditions used. During this phase, nucleation of small clusters from protein monomers are slowly formed (Yousaf et al., 2017; Liu et al., 2018). During the elongation phase, ThT fluorescence intensity increased rapidly indicating the quick aggregation of small clusters into amyloid fibrils. After 1-day incubation, the fluorescence intensity reached a maximum value and gradually stabilized, which demonstrated a saturation phase with the formation of mature fibrils. When incubated with BPQDs, the evolution of ThT fluorescence in denatured insulin solutions was dramatically changed. Several concentrations of BPQDs at 100, 200, and 500 ng/mL were found to totally resist the aggregation kinetics as denoted by the almost no increase in the ThT fluorescence intensity after 4 days. Even when exposed to an ultralow concentration of 50 ng/mL BPQDs (red line), a significant inhibition of insulin fibrils could be observed. The lag phase was extended to about 2.5 days and the fluorescence intensity at the final saturation phase was 60%, lower than that of insulin alone. BPQDs alone were also incubated with ThT under the same conditions to identify if the observations could have resulted from an interaction between ThT and BPQDs. As shown in Figure S1, no change in emission fluorescence was found over several days, ruling out any possible artifact from ThT and BPQDs interactions. Therefore, insulin fibrillation was effectively suppressed by BPQDs at concentrations that are much lower than previously reported from other nanomaterials (Table 1). Contrary to gold nanoparticles, whose inhibitory concentration was reported to be as low as 1 nM, BPQDs do not need to be functionalized with peptides or other functional groups (Mirsadeghi et al., 2015; Ruff et al., 2018; Xiong et al., 2017; Yin et al., 2016), or to be remotely activated (Li et al., 2017) to maintain an exceptionally high inhibitory effect.

During the aggregation process, the secondary structure of insulin was monitored using far-UV CD spectra. As shown in Figure 1B, two negative peaks were identified at 208 and 222 nm at the initial incubation of insulin, indicating the presence of α-helix conformation. After 24 h incubation of insulin alone, the negative peak intensity decreased and a single broad negative peak was observed at 218 nm, indicating that most of the secondary structure was converted to β-sheet conformation. Quantitatively, analysis of the fractional secondary structure (Figure 1C) showed that the α-helix conformation decreased from 32.5% to 0.0%
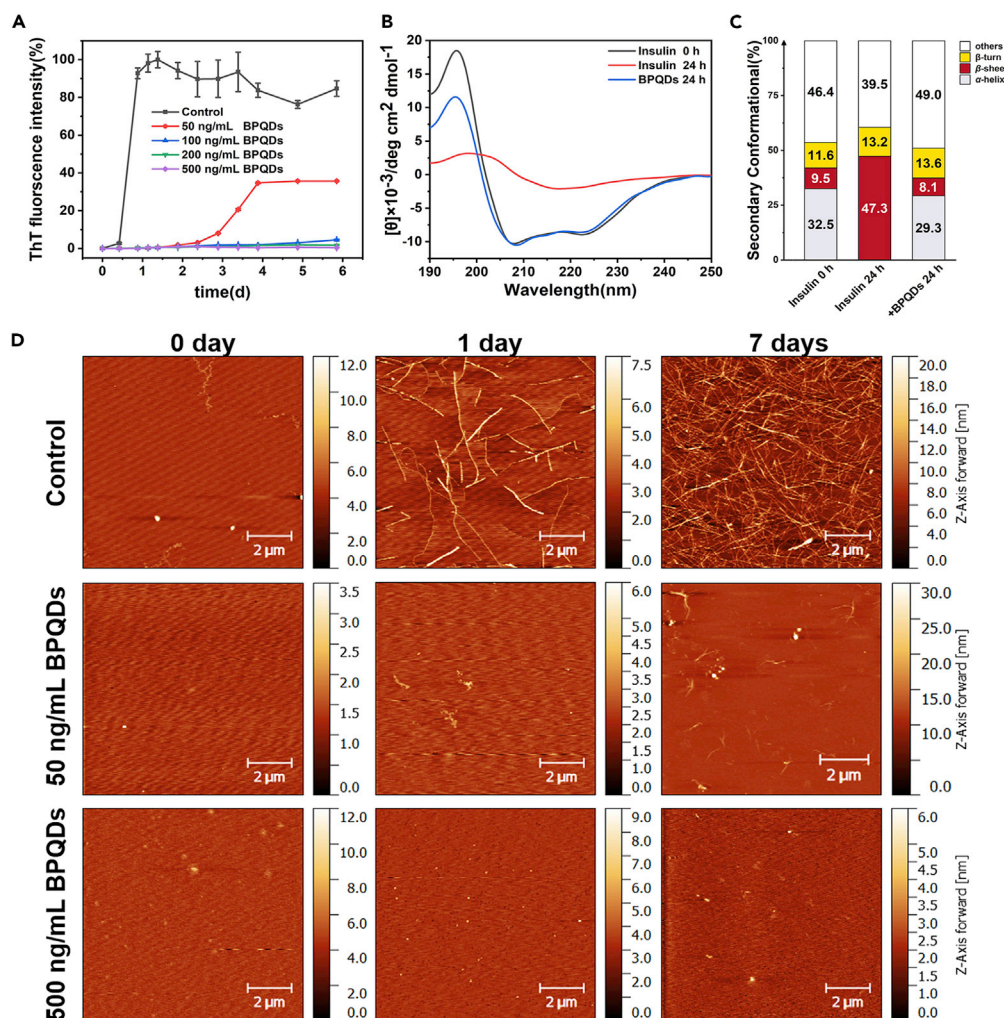
Figure 1. Influence of BPQDs on the Inhibition of Insulin Fibrillation Aggregation

(A) The growth kinetic curves of insulin amyloid fibrillation monitored by ThT fluorescence assay. Relative ThT fluorescence intensity varied at 485 nm with the incubation time of insulin at different BPQDs concentrations (0, 50, 100, 200, 500 ng/mL). The final concentration of insulin is 2 mg/mL. All data represent the average from three experiments. Error bars indicate ± SD.

(B) Far-UV CD spectra curves of insulin alone and in the presence of 500 ng/mL of BPQDs, as well as the corresponding secondary structure content.

(C) The primal insulin and the incubated (24 h) insulin were diluted twice and tested using a 1-nm quartz cell.

(D) AFM images of insulin amyloid fibrillation at different incubation times (0, 1, and 7days) for insulin alone and insulin-BPQDs (50 and 500 ng/mL) solutions. (AFM: tapping mode).

and the β-sheet conformation increased from 9.5% to 47.3%. Co-incubation of insulin with BPQDs (500 ng/mL) proves that the two negative peaks observed at 208 and 222 nm in insulin solutions alone at t = 0 still remains after 24 h, demonstrating that the α-helical secondary structure was still present. After the addition of BPQDs, a small variation in the α-helix (from 32.5% to 29.3%) and the β-sheet (from 9.5% to 8.1%) fractions was detected, showing that only a small part of the α-helix and the β-sheet conformation evolved into other conformations such as random coil. These observations confirmed that the inhibitory effect of BPQDs is due to their capacity to stabilize the α-helix secondary structure of insulin, an ability that must involve specific interactions between the nanomaterial and the protein.

To further explore the inhibitory effect of BPQDs on insulin amyloid fibrillation, the morphology of insulin protofibrils at different incubation times (0, 1, and 7 days) was followed by AFM. As shown in Figure 1D,

Protein	Protein Concentration (mg/mL)	Inhibitor	Inhibitor Concentration (ng/mL)	Mass Ratios (Inhibitor: Protein)	Inhibition rate[a] (%)	Reference
Insulin	2.000	Black phosphorus quantum dots	100	1:20000	95	This work
	2.000	Silicon nanoparticles	5,000	1:400	88	Ma et al., 2019
	0.200	Carbon dots	10,000	1:20	27	Li et al., 2015
HIAPP	0.077	Fluorinated graphene quantum dots	385,000	1:0.2	95	Yousaf et al., 2017
	0.096	Graphene quantum dots	500,000	1:0.2	60	Wang et al., 2018b
Aβ	0.087	Au nanoclusters	20,000	1: 4.3	95	Gao et al., 2017
	0.181	bPEI-coated carbon dots	500,000	1:0.4	75	Chung et al., 2017
α-syn	5.000	Graphene quantum dots	5,000,000	1:1	90	Kim et al., 2018

Table 1. Summary of the Mass Concentration Ratios of Inhibitors and Amyloid Protein

For comparison, the protein and inhibitor concentrations were, respectively, converted to mass concentration.

[a]The inhibition rate is estimated based on the results of ThT fluorescence spectroscopy.

during incubation of insulin alone, a few long fibrils appeared after 1 day, whereas numerous mature fibrils were observed after 7 days. When insulin was co-incubated with 50 ng/mL of BPQDs, only a few short fibrils were detected after 7 days of incubation. When 500 ng/mL of BPQDs was used, no fibrils were detected after 7 days of incubation. Therefore, AFM data were fully consistent with the results obtained from the ThT fluorescence assay and CD spectra, further confirming the excellent capability of BPQDs in inhibiting insulin aggregation.

To further understand the inhibitory mechanism of BPQDs, insulin solutions were exposed to 500 ng/mL BPQDs at different stages of the aggregation process (0, 10, 24, 35, and 48 h) and ThT signal was monitored. As shown in Figures 2A and 2B, during the lag phase (0 and 10 h), the addition of BPQDs completely inhibited insulin fibrillation as demonstrated by the absence of variation in the ThT signal. When BPQDs were introduced during the elongation phase (24, 35, and 48 h), ThT fluorescence intensity decreased, indicating a loss of β-sheet structure and therefore depolymerization of protofibrils. These results suggested that BPQDs could bind not only to insulin monomers to interfere with the early stages of nucleation, but also to fibrils and stop their growth. Therefore, BPQDs have a broad impact on amyloid inhibition on various stages of the aggregation process, especially in the lag phase where almost complete inhibition was observed.

Since amyloid fibrillation kinetics is highly sensitive to ionic strength, a kinetic test was also performed in the absence of ions in the insulin solution (Figure 2C). Even though the kinetics of fibrillation was dramatically slowed (insulin alone took about 15 days to reach the saturation phase), BPQDs were still found to inhibit fibrillation completely at concentrations as low as 250 ng/mL.

Depolymerization Assay of Insulin Fibrils by BPQDs

Considering the capacity of BPQDs to reduce the concentration/length of amyloid fibers during the elongation phase, the effect of BPQDs on mature fibrils was further examined in the saturation phase (Figure 3). Insulin monomer was first incubated for 4 days to ensure complete conversion to mature fibrils (Figure 3B). Then an equal amount of ultrapure water (control group) and 500 ng/mL BPQDs were added separately
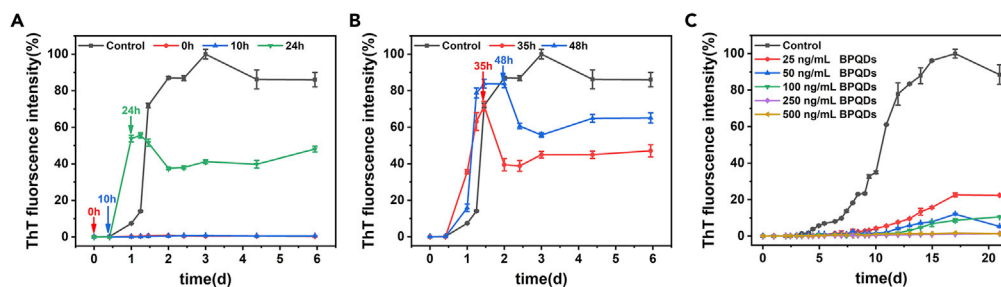
Figure 2. ThT Fluorescence Intensity of Insulin Amyloid Fibrillation for Analyzing the Effect of BPQDs Added Time and the Existence of NaCl

The black line was treated as a control experiment that no BPQDs have been added. BPQDs (500 ng/mL) were added at different incubation times, including (A) 0 (red), 10 (blue), 24 (green), (B) 35 (red), and 48 h (blue), respectively. Arrows indicate the time of BPQDs added. All data represent the average from three experiments. Error bars indicate ± SD. (C) The growth kinetic curves of insulin under incubation conditions without NaCl monitored by ThT fluorescence assay. Relative ThT fluorescence intensity at 485 nm varied as a function of incubation time of insulin in the presence of various concentrations (0, 25, 50, 100, 250, 500 ng/mL) of BPQDs. All data represent the average from three experiments. Error bars indicate ± SD.

and ThT fluorescence was monitored. As shown in Figure 3A, the ThT fluorescence intensity gradually decreased almost 60% in the presence of BPQDs after 1-day incubation. Only short and thick fibers were observed by AFM imaging, confirming that long fibrils originally present have totally disappeared from the suspension (Figure 3C). These results confirmed the capacity of BPQDs to depolymerize mature fibers, in addition to stop their growth.

Elucidation of the Interaction between BPQDs and Insulin by Molecular Dynamics Simulation

To obtain insights at the molecular level on the unique capacity of BPQDs to inhibit insulin amyloid fibrillation, MD simulations of insulin/BPQDs aggregates were performed. Since insulin fibrils are mainly formed from monomers, interaction between a single insulin molecule and a BPQD was first studied (Ahmad et al., 2005). The time evolution of root-mean-square deviation (RMSD) (Figure S2) confirmed that the BPQD/insulin complex became stable after about 40 ns, and we concentrate our analysis on the last 10 ns. Figures 4A–4D show the structures of insulin alone and in presence of BPQDs before and after 60 ns of simulation. In the absence of BPQDs, the native α-helix structure of insulin partially transformed into β conformation after 60 ns (brown segment in Figure 4C, accounting for 7.61%), which contributed to form β-sheets. Inversely, the presence of BPQDs showed to effectively maintain the α-helix structure, as no β conformation could be seen during the simulation.

The B12–B17 segment of insulin is normally regarded as the main segment forming the spine of the fibril via anti-parallel β-strands (Groenning et al., 2009). To gain a deeper understanding of the depolymerization process of amyloid fibrils by BPQDs, the evolution of the structure of the B12–B17 (VEALYL) fragment was investigated in the presence of BPQDs. As shown in Figures 4E and 4G, the double β-strand structure of the fragment was preserved during the whole duration of the simulation when no BPQD was present. When BPQD was introduced in the simulation, BPQD was able to disrupt the β-sheets totally in the time frame of the simulation (Figures 4F and 4H).

Specifically, BPQDs interact with 16 binding sites of insulin and most of them possessed the hydrophobic residues (Ile, Phe, Leu, Tyr, and Val). There are some useful ways to visually study inter-fragment and intra-fragment interactions, and we did the weak interaction analysis with Independent Gradient Model (ICG) (Lefebvre et al., 2017) by Multiwfn, a multifunctional wave function analyzer (Lu and Chen, 2012). The green isosurface in Figure S3 represents the van der Waals' force region between a BPQD and an asparagine. For the depolymerization process, the solvent accessible surface area (SASA) of the β-sheet fragment (Figure S4A) indicates that this fragment becomes less hydrophobic after binding with BPQDs and the hydrophobic interactions attribute to the depolymerization force. At the same time, the hydrogen bonds between the β-sheet fragment and water increase, which is consistent with the SASA results (Figure S4B). The van der Waals' force region between a BPQD and β-sheet fragment (Figure S5) demonstrates that
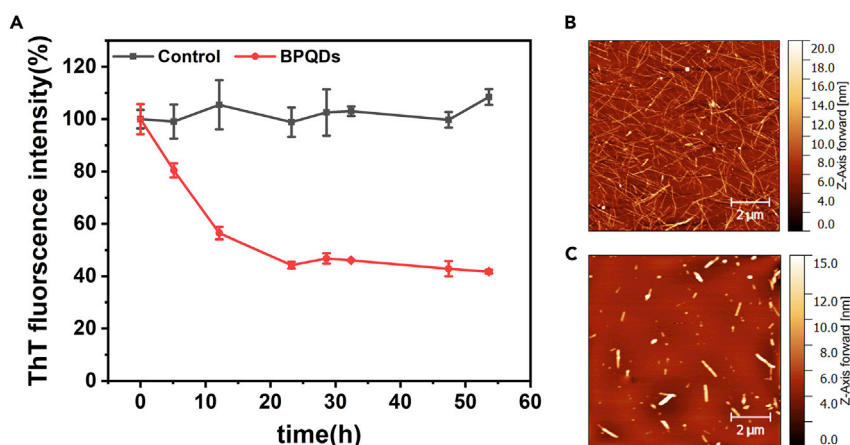
Figure 3. Depolymerization Assay

(A) ThT fluorescence intensity in insulin solutions in absence (black) and presence (red) of BPQDs. BPQDs (500 ng/mL) were added after 5 days of fibrils maturation. Starting time (t = 0) corresponds to the instant when BPQDs were added to the mature fibrils suspension. All data points represent the average from three independent experiments. Error bars indicate ± SD.

(B and C) (B) AFM images of insulin alone after 2 days incubation, as well as the co-incubation of insulin and BPQDs (C).

both the inhabitation and dissociation are driven chiefly by hydrophobic interactions and van der Waals' force, accompanied by structural changes.

The Effect of BPQDs on Amyloid Cytotoxicity

To evaluate the effect of BPQDs on amyloid-induced cytotoxicity, PC12 cells were assayed using the 3-(4,5-dimethylthiazol-2-yl)-2,5-diphenyltetrazolium bromide (MTT) assay to assess cellular activity. As shown in Figure 5, compared with the control test (addition of buffer), cell viability was decreased to 58% in the presence of the insulin fibrils solutions, which indicates strong cytotoxicity. However, under the same incubation conditions, the cellular activity of BPQDs alone was similar to the control test (about 97.5%), which further verified the non-toxicity of BPQDs and their potential application in the biological field. In addition, cellular activity was maintained at levels similar to that of control (95% or more of cell viability) in the co-incubated solutions of insulin and BPQDs, which illustrated the ability of BPQDs in reducing amyloid-induced cytotoxicity. The reasons for such dramatic effect was attributed to the inhibition of insulin aggregation by BPQDs, as well as the non-toxic and physical property of BPQDs (Chen et al., 2017; Luo et al., 2019; Shao et al., 2016; Sun et al., 2016).

DISCUSSION

The BPQDs can make up a drug delivery system with pH/photoresponsive release properties, and the outstanding *in vivo* antitumor therapeutic outcome was realized after the synergistic photodynamic/photothermal/chemotherapy with BPQDs (Chen et al., 2017). Aiming at the therapy of diseases involving protein fibrillation, we synthesize BPQDs and found it inhibits insulin aggregation completely even in a very low concentration, 50 ng/mL, which appeared as the lowest concentration of nano-inhibitor reported so far. Interestingly, compared with other nano materials, such as SiNPs and carbon dots, BPQDs had a more outstanding effect on suppressing insulin fibrillation in the lag phase, elongation phase, and saturation phase at this concentration. Furthermore, BPQDs not only inhibit insulin monomer and protofibrils further aggregation, but also depolymerize protofibrils and even mature fibers.

Molecular dynamics simulations demonstrate that BPQDs interact with insulin mainly through hydrophobic and van der Waals' interactions and the binding sites (Ile, Phe, Leu, Tyr, and Val) reserve the initial configuration of insulin, which resists the transformation from α-helix structure to β-sheet structure and open the formed β-sheet fragments. In contrast, without BPQDs, the native α-helix structure of insulin partially transformed into β conformation, which contributed to form β-sheets. BPQDs also contribute to the depolymerization process of amyloid fibrils. MD simulations reveal that BPQDs disrupt the β-strand structure of the main segment forming the spine of the fibril by interacting with individual chains and separating them.
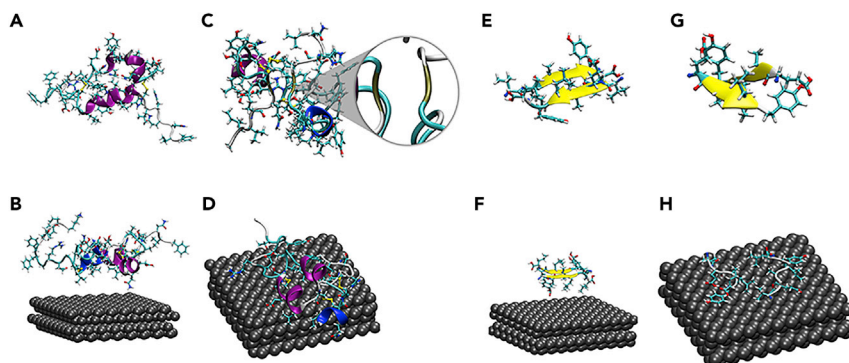
Figure 4. Molecular Dynamics Simulation

(A) Initial structure of pure insulin.

(B) Initial structure of insulin with the BPQDs.

(C) Final structure of pure insulin after 60 ns. The enlarged brown part represents the β conformation.

(D) Final structure of insulin with the BPQDs after 60 ns.

(E) Initial β-sheet structure formed by two insulin parts (B12–B17) without BPQDs.

(F) Initial structure of the same fragment insulin (B12–B17) with the BPQDs.

(G) Final β-sheet structure formed by two insulin parts (B12–B17) without BPQDs after 60 ns.

(H) Final structure of the same fragment (B12–B17) with the BPQDs after 60 ns.

Furthermore, without BPQDs, the C-terminal fragment of the chain B of insulin is not well ordered, which leads to the exposure of its non-polar areas, and the aromatic side chains (B24–B26, FFY) may contribute to the formation of non-native β-sheet, which resists the fibrillation (Hua and Weiss, 2004). In contrast, the aromatic ring of B24–B26 (Figure S6) was able to bind to the BPQDs and avoid the formation of β-sheets. As a consequence, in the presence of BPQDs, α-helix domains remain more stable, which stops the formation of fibrils. Upon fibrillation, insulin undergoes structural changes from a predominantly α-helical state to a β-sheet-rich conformation (Ivanova et al., 2009), but BPQDs could restrain this process by interacting with the insulin.

To explore the difference from other nanomaterials, we also performed the MD simulation for insulin and silica nanoparticles (SiNPs). Differing from BPQDs, which mainly interact with insulin by dispersion force and hydrophobic interaction, electrostatic interaction and hydrogen bond are the primary driving forces to combine the negatively charged SiNPs surface and insulin (Figures S7 and S8). Most residues of insulin are hydrophobic or neutral groups, and there are more binding sites of insulin on BPQDs than SiNPs, leading to that the BPQDs could inhibit insulin aggregation completely in a surprisingly lower concentration than SiNPs.

Cytotoxicity experiments suggested that BPQDs can reduce insulin-induced cytotoxicity. Compared with other nano-inhibitors, BPQDs demonstrate non-toxicity and very high inhibition efficiency. Therefore, BPQDs have great potential in the prevention and treatment of amyloidosis, as well as storage and processing of proteins in the pharmaceutical industry.

Limitations of the Study

Owing to the limitation of experimental conditions, the inhibition effect of BPQDs on insulin aggregation was not performed *in vivo*. Although the insulin incubation process was similar to that in other previous works (high temperature or high salinity), it could not demonstrate that the BPQDs possess the ability of inhibiting insulin amyloid. Thus, it is necessary to establish an *in vivo* mode in the future experiments. In addition, the interaction mechanism of BPQDs and insulin or denatured insulin should be stated in greater detail, such as the binding site or spatial structure effect. All of these will be needed for a further study to help us understand the inhibition or promotion mechanism of nanomaterials on protein amyloidosis.

METHODS

All methods can be found in the accompanying Transparent Methods supplemental file.
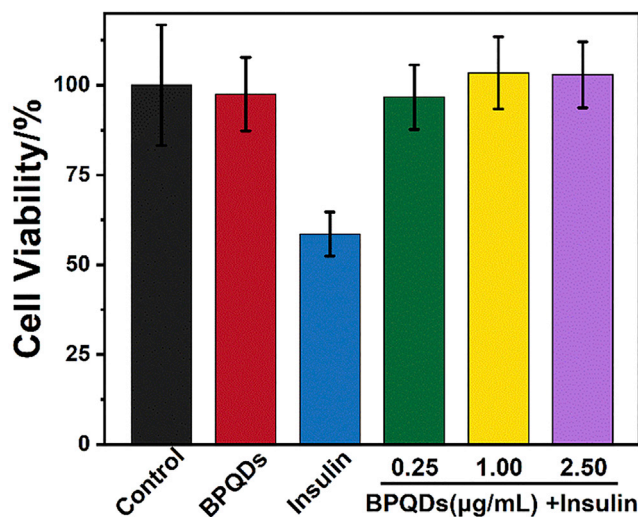
Figure 5. Cell Toxicity Assay of PC12 Cells

Cell viability was measured by the MTT reduction method. PC12 cells were treated with BPQDs alone, insulin alone, and insulin in the presence of BPQDs after 5 days incubation. The concentrations of BPQDs were 0.25, 1.00, and 2.50 μg/mL, respectively. The final concentration of insulin was 5 μM. The control experiment was treated without insulin fibrils. All data represent the average from six different data. Error bars indicate ± SD.

DATA AND CODE AVAILABILITY

All data are available from the corresponding author upon reasonable request.

SUPPLEMENTAL INFORMATION

Supplemental Information can be found online at https://doi.org/10.1016/j.isci.2020.101044.

AUTHOR CONTRIBUTIONS

S.W. and R.S. conceived and designed the experiments. S.W. and Y.X. carried out the experiments. C.L. performed the computations. S.W., C.L., Y.X., X.B., and R.S. drafted the manuscript, and all authors participated in the writing and review of the final draft.

DECLARATION OF INTERESTS

The authors have no conflicts of interest to declare.

REFERENCES

Ahmad, A., Uversky, V.N., Hong, D., and Fink, A.L. (2005). Early events in the fibrillation of monomeric insulin. J. Biol. Chem. *280*, 42669–42675.

Biancalana, M., and Koide, S. (2010). Molecular mechanism of thioflavin-T binding to amyloid fibrils. Biochim. Biophys. Acta *1804*, 1405–1412.

Cabaleiro-Lago, C., Quinlan-Pluck, F., Lynch, I., Dawson, K.A., and Linse, S. (2010). Dual effect of amino modified polystyrene nanoparticles on amyloid β protein fibrillation. ACS Chem. Neurosci. *1*, 279–287.

Chen, W., Ouyang, J., Liu, H., Chen, M., Zeng, K., Sheng, J., Liu, Z., Han, Y., Wang, L., Li, J., et al.

(2017). Black phosphorus nanosheet-based drug delivery system for synergistic photodynamic/photothermal/chemotherapy of cancer. Adv. Mater. *29*, 1603864.

Chen, W., Ouyang, J., Yi, X., Xu, Y., Niu, C., Zhang, W., Wang, L., Sheng, J., Deng, L., Liu, Y.N., et al. (2018). Black phosphorus nanosheets as a

neuroprotective nanomedicine for neurodegenerative disorder therapy. Adv. Mater. 30, 1703458.

Chiti, F., and Dobson, C.M. (2006). Protein misfolding, functional amyloid, and human disease. Annu. Rev. Biochem. 75, 333–366.

Choi, J.R., Yong, K.W., Choi, J.Y., Nilghaz, A., Lin, Y., Xu, J., and Lu, X. (2018). Black phosphorus and its biomedical applications. Theranostics 8, 1005–1026.

Chung, Y.J., Kim, K., Lee, B.I., and Park, C.B. (2017). Carbon nanodot-sensitized modulation of alzheimer's β-amyloid self-assembly, disassembly, and toxicity. Small 13, 1700983.

Eisenberg, D., and Jucker, M. (2012). The amyloid state of proteins in human diseases. Cell 148, 1188–1203.

Gao, G., Zhang, M., Gong, D., Chen, R., Hu, X., and Sun, T. (2017). The size-effect of gold nanoparticles and nanoclusters in the inhibition of amyloid-β fibrillation. Nanoscale 9, 4107–4113.

Goedert, M., and Spillantini, M.G. (2006). A century of Alzheimer's disease. Science 314, 777–781.

Groenning, M., Frokjaer, S., and Vestergaard, B. (2009). Formation mechanism of insulin fibrils and structural aspects of the insulin fibrillation process. Curr. Protein Pept. Sci. 10, 509–528.

Hua, Q.X., and Weiss, M.A. (2004). Mechanism of insulin fibrillation: the structure of insulin under amyloidogenic conditions resembles a protein-folding intermediate[J]. J. Biol. Chem. 279, 21449–21460.

Ivanova, M.I., Sievers, S.A., Sawaya, M.R., Wall, J.S., and Eisenberg, D. (2009). Molecular basis for insulin fibril assembly[J]. Proc. Natl. Acad. Sci. U S A 106, 18990–18995.

Jeevanandam, J., Barhoum, A., Chan, Y.S., Dufresne, A., and Danquah, M.K. (2018). Review on nanoparticles and nanostructured materials: history, sources, toxicity and regulations. Beilstein J. Nanotechnol. 9, 1050–1074.

Kim, D., Yoo, J.M., Hwang, H., Lee, J., Lee, S.H., Yun, S.P., Park, M.J., Lee, M., Choi, S., Kwon, S.H., et al. (2018). Graphene quantum dots prevent α-synucleinopathy in Parkinson's disease. Nat. Nanotechnol. 13, 812–818.

Lee, C.C., Nayak, A., Sethuraman, A., Belfort, G., and Mcrae, G.J. (2007). A three-stage kinetic model of amyloid fibrillation. Biophys. J. 92, 3448–3458.

Lee, J., Culyba, E.K., Powers, E.T., and Kelly, J.W. (2011). Amyloid-β forms fibrils by nucleated conformational conversion of oligomers. Nat. Chem. Biol. 7, 602–609.

Lefebvre, C., Rubez, G., Khartabil, H., Boisson, J.C., Contreras-Garcia, J., and Henon, E. (2017). Accurately extracting the signature of intermolecular interactions present in the NCI plot of the reduced density gradient versus electron density. Phys. Chem. Chem. Phys. 19, 17928–17936.

Li, M., Yang, X., Ren, J., Qu, K., and Qu, X. (2012). Using graphene oxide high near-infrared

absorbance for photothermal treatment of Alzheimer's disease. Adv. Mater. 24, 1722–1728.

Li, S., Wang, L., Chusuei, C.C., Suarez, V.M., Blackwelder, P.L., Micic, M., Orbulescu, J., and Leblanc, R.M. (2015). Nontoxic carbon dots potently inhibit human insulin fibrillation. Chem. Mater. 27, 1764–1771.

Li, Y., Du, Z., Liu, X., Ma, M., Yu, D., Lu, Y., Ren, J., and Qu, X. (2019). Near-infrared activated black phosphorus as a nontoxic photo-oxidant for Alzheimer's amyloid-β peptide. Small 15, 1901116.

Li, M., Guan, Y., Zhao, A., Ren, J., and Qu, X. (2017). Using multifunctional peptide conjugated Au nanorods for monitoring β-amyloid aggregation and chemo-photothermal treatment of Alzheimer's disease. Theranostics 7, 2996–3006.

Lim, Y.J., Zhou, W.H., Li, G., Hu, Z.W., Hong, L., Yu, X.F., and Li, Y.M. (2019). Black phosphorus nanomaterials regulate the aggregation of amyloid-β. ChemNanoMat 5, 606–611.

Linse, S., Cabaleiro-Lago, C., Xue, W.F., Lynch, I., Lindman, S., Thulin, E., Radford, S.E., and Dawson, K.A. (2007). Nucleation of protein fibrillation by nanoparticles. Proc. Natl. Acad. Sci. U S A 104, 8691–8696.

Liu, Y., Xu, L.P., Dai, W., Dong, H., Wen, Y., and Zhang, X. (2015). Graphene quantum dots for the inhibition of β amyloid aggregation. Nanoscale 7, 19060–19065.

Liu, Y., Xu, L.P., Wang, Q., Yang, B., and Zhang, X. (2018). Synergistic inhibitory effect of GQDs-tramiprosate covalent binding on amyloid aggregation. ACS Chem. Neurosci. 9, 817–823.

Lu, T., and Chen, F. (2012). Multiwfn: a multifunctional wavefunction analyzer. J. Comput. Chem. 33, 580–592.

Luo, M., Fan, T., Zhou, Y., Zhang, H., and Mei, L. (2019). 2D Black phosphorus–based biomedical applications. Adv. Funct. Mater. 29, 1808306.

Ma, Y., Huang, R., Qi, W., Su, R., and He, Z. (2019). Fluorescent silicon nanoparticles inhibit the amyloid fibrillation of insulin. J. Mater. Chem. B 7, 1397–1403.

Mirsadeghi, S., Dinarvand, R., Ghahremani, M.H., Hormozi-Nezhad, M.R., Mahmoudi, Z., Hajipour, M.J., Atyabi, F., Ghavami, M., and Mahmoudi, M. (2015). Protein corona composition of gold nanoparticles/nanorods affects amyloid β fibrillation process. Nanoscale 7, 5004–5013.

Niu, L., Liu, L., Xi, W., Han, Q., Li, Q., Yu, Y., Huang, Q., Qu, F., Xu, M., Li, Y., et al. (2016). Synergistic inhibitory effect of peptide-organic coassemblies on amyloid aggregation. ACS Nano 10, 4143–4153.

Petkova, A.T., Leapman, R.D., Guo, Z.H., Yau, W.M., Mattson, M.P., and Tycko, R. (2005). Self-propagating, molecular-level polymorphism in Alzheimer's β-amyloid fibrils. Science 307, 262–265.

Pike, C.J., Burdick, D., Walencewicz, A.J., Glabe, C.G., and Cotman, C.W. (1993). Neurodegeneration induced by β-amyloid

peptides in vitro: the role of peptide assembly state. J. Neurosci. 13, 1676–1687.

Ratha, B.N., Ghosh, A., Brender, J.R., Gayen, N., Ilyas, H., Neeraja, C., Das, K.P., Mandal, A.K., and Bhunia, A. (2016). Inhibition of insulin amyloid fibrillation by a novel amphipathic heptapeptide: mechanistic details studied by spectroscopy in combination with microscopy. J. Biol. Chem. 291, 23545–23556.

Ruff, J., Hassan, N., Morales-Zavala, F., Steitz, J., Araya, E., Kogan, M.J., and Simon, U. (2018). CLPFFD–PEG functionalized NIR-absorbing hollow gold nanospheres and gold nanorods inhibit β-amyloid aggregation. J. Mater. Chem. B 6, 2432–2443.

Shao, J., Xie, H., Huang, H., Li, Z., Sun, Z., Xu, Y., Xiao, Q., Yu, X.F., Zhao, Y., Zhang, H., et al. (2016). Biodegradable black phosphorus-based nanospheres for in vivo photothermal cancer therapy. Nat. Commun. 7, 12967.

Shulman, J.M., De Jager, P.L., and Feany, M.B. (2011). Parkinson's disease: genetics and pathogenesis. Annu. Rev. Pathol. 6, 193–222.

Sun, C., Wen, L., Zeng, J., Wang, Y., Sun, Q., Deng, L., Zhao, C., and Li, Z. (2016). One-pot solventless preparation of PEGylated black phosphorus nanoparticles for photoacoustic imaging and photothermal therapy of cancer. Biomaterials 91, 81–89.

Thakur, G., Micic, M., Yang, Y., Li, W., Movia, D., Giordani, S., Zhang, H., and Leblanc, R.M. (2011). Conjugated quantum dots inhibit the amyloid β (1-42) fibrillation process. Int. J. Alzheimers Dis. 2011, 502386.

Walker, F.O. (2007). Huntington's disease. Lancet 369, 218–228.

Wang, S.T., Lin, Y., Todorova, N., Xu, Y., Mazo, M., Rana, S., Leonardo, V., Amdursky, N., Spicer, C.D., Alexander, B.D., et al. (2017). Facet-dependent interactions of islet amyloid polypeptide with gold nanoparticles: implications for fibril formation and peptide-induced lipid membrane disruption. Chem. Mater. 29, 1550–1560.

Wang, M., Liang, Y., Liu, Y., Ren, G., Zhang, Z., Wu, S., and Shen, J. (2018a). Ultrasmall black phosphorus quantum dots: synthesis, characterization, and application in cancer treatment. Analyst 143, 5822–5833.

Wang, M., Sun, Y., Cao, X., Peng, G., Javed, I., Kakinen, A., Davis, T.P., Lin, S., Liu, J., Ding, F., et al. (2018b). Graphene quantum dots against human IAPP aggregation and toxicity in vivo. Nanoscale 10, 19995–20006.

Wang, J., Zhang, Z., Zhang, H., Li, C., Chen, M., Liu, L., and Dong, M. (2019). Enhanced photoresponsive graphene oxide-modified g-C₃N₄ for disassembly of amyloid β fibrils. ACS Appl. Mater. Interfaces 11, 96–103.

Wu, W.H., Sun, X., Yu, Y.P., Hu, J., Zhao, L., Liu, Q., Zhao, Y.F., and Li, Y.M. (2008). TiO₂ nanoparticles promote β-amyloid fibrillation in vitro. Biochem. Biophys. Res. Commun. 373, 315–318.

Wu, D., Ma, Y., Cao, Y., and Zhang, T. (2020). Mitochondrial toxicity of nanomaterials. Sci. Total Environ. 702, 134994.

Xia, Y., Wang, S., Huang, R., Su, R., Qi, W., and He, Z. (2018). Adsorption-desorption behavior of black phosphorus quantum dots on mucin surface. Langmuir *34*, 8508–8515.

Xiao, L., Zhao, D., Chan, W.H., Choi, M.M., and Li, H.W. (2010). Inhibition of β 1-40 amyloid fibrillation with N-acetyl-L-cysteine capped quantum dots. Biomaterials *31*, 91–98.

Xiong, N., Zhao, Y., Dong, X., Zheng, J., and Sun, Y. (2017). Design of a molecular hybrid of dual peptide inhibitors coupled on AuNPs for enhanced inhibition of amyloid β-protein aggregation and cytotoxicity. Small *13*, 1601666.

Yan, M., Zhang, Y., Xu, K., Fu, T., Qin, H., and Zheng, X. (2011). An in vitro study of vascular endothelial toxicity of CdTe quantum dots. Toxicology *282*, 94–103.

Yang, B., Chen, Y., and Shi, J. (2019). Nanocatalytic medicine. Adv. Mater. *31*, 1901778.

Yin, T., Xie, W., Sun, J., Yang, L., and Liu, J. (2016). Penetratin peptide-functionalized gold nanostars: enhanced BBB permeability and NIR photothermal treatment of Alzheimer's disease using ultralow irradiance. ACS Appl. Mater. Interfaces *8*, 19291–19302.

Yoo, S.I., Yang, M., Brender, J.R., Subramanian, V., Sun, K., Joo, N.E., Jeong, S.H., Ramamoorthy, A., and Kotov, N.A. (2011). Inhibition of amyloid peptide fibrillation by inorganic nanoparticles: functional similarities with proteins. Angew. Chem. Int. Ed. *50*, 5110–5115.

Yousaf, M., Huang, H., Li, P., Wang, C., and Yang, Y. (2017). Fluorine functionalized graphene quantum dots as inhibitor against hIAPP amyloid aggregation. ACS Chem. Neurosci. *8*, 1368–1377.

Zhang, T., Wan, Y., Xie, H., Mu, Y., Du, P., Wang, D., Wu, X., Ji, H., and Wan, L. (2018). Degradation chemistry and stabilization of exfoliated few-layer black phosphorus in water. J. Am. Chem. Soc. *140*, 7561–7567.

Zhang, S., Zhang, X., Lei, L., Yu, X.F., Chen, J., Ma, C., Wu, F., Zhao, Q., and Xing, B. (2019). pH-Dependent degradation of layered black phosphorus: essential role of hydroxide ions. Angew. Chem. Int. Ed. *58*, 467–471.

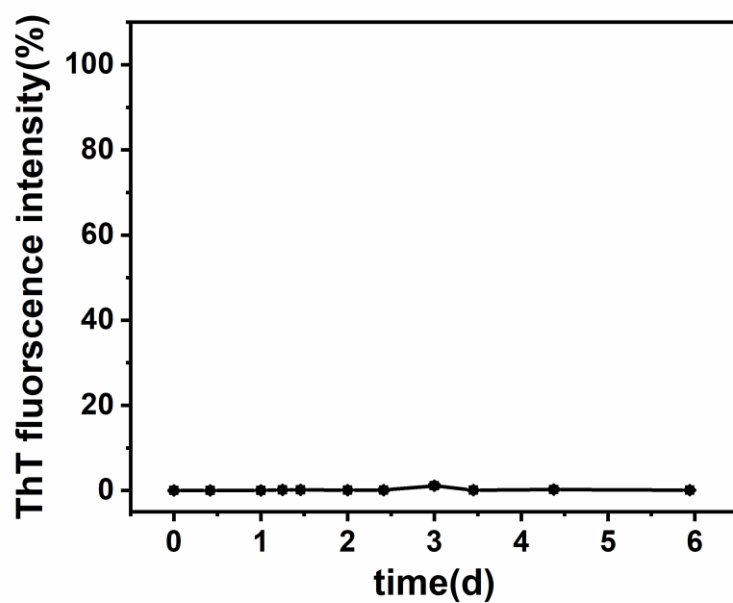# Supplemental Information

# Nontoxic Black Phosphorus Quantum Dots

Inhibit Insulin Amyloid Fibrillation

at an Ultralow Concentration

Siqi Wang, Chuanxi Li, Yinqiang Xia, Shaohuang Chen, Jordan Robert, Xavier Banquy, Renliang Huang, Wei Qi, Zhimin He, and Rongxin Su

**Figure S1.** ThT fluorescence intensity of BPQDs (500 ng/mL) alone as a function of incubation time.

All data represent the average from three experiments. Error bars indicate ±SD. Related to Figure 1A.
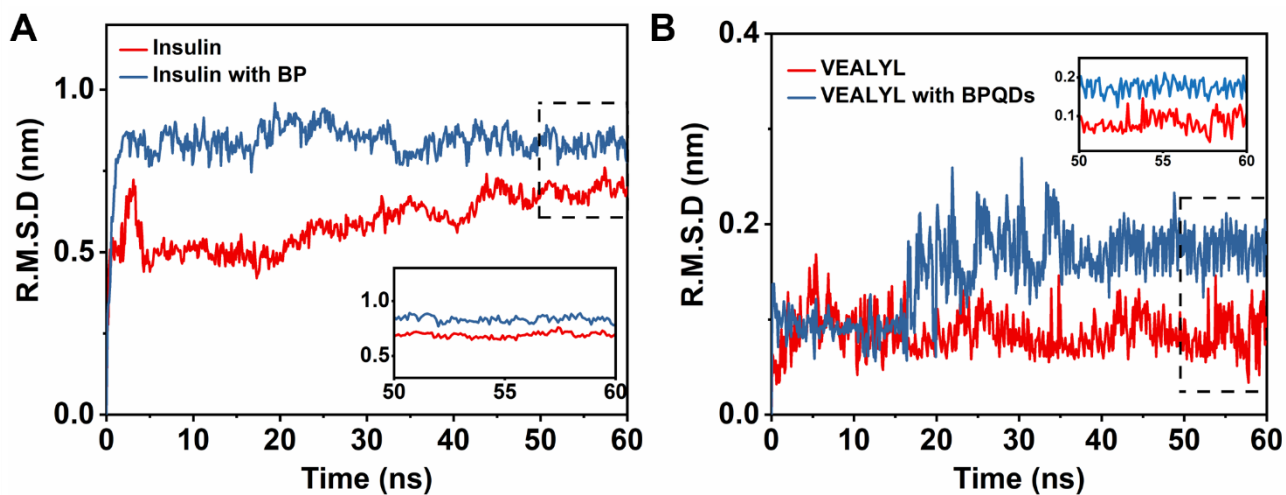
Figure S2. The R.M.S.D. varying with time of different systems. (a) The R.M.S.D. of pure insulin and insulin with BPQDs. **(b)** The R.M.S.D. of β-sheet fragment (B12-B17, VEALYL) of pure insulin and β-sheet fragment with BPQDs. Related to Figure 4.
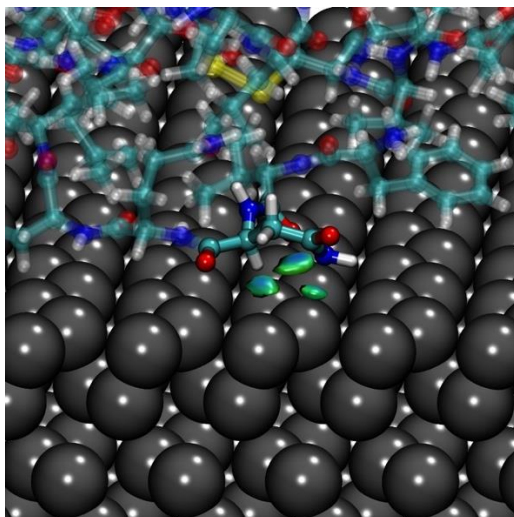
Figure S3. The Van der Waals' force between the BPQDs and asparagine. The green dot area indicate the Van der Waals' force positions. Related to Figure 4.
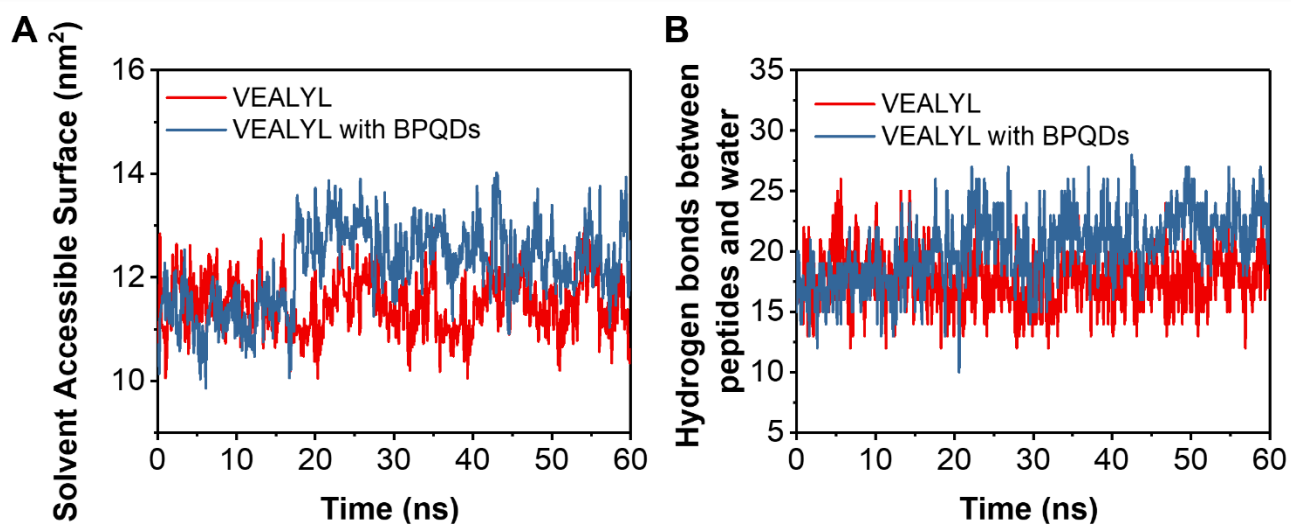
Figure S4. The **(a)** solvent accessible surface and **(b)** hydrogen bonds between β-sheet fragment (B12-B17, VEALYL) and water varying with time of different systems. Related to Figure 4.
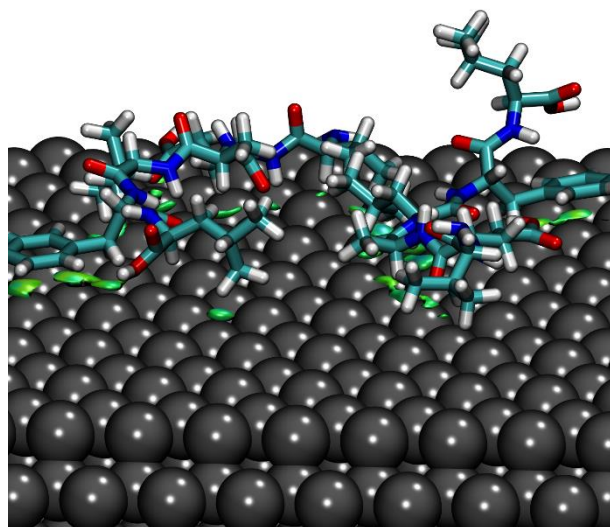
Figure S5. The Van der Waals' force between the BPQDs and β-sheet fragment (B12-B17, VEALYL). The green dot area indicate the Van der Waals' force positions. Related to Figure 4.
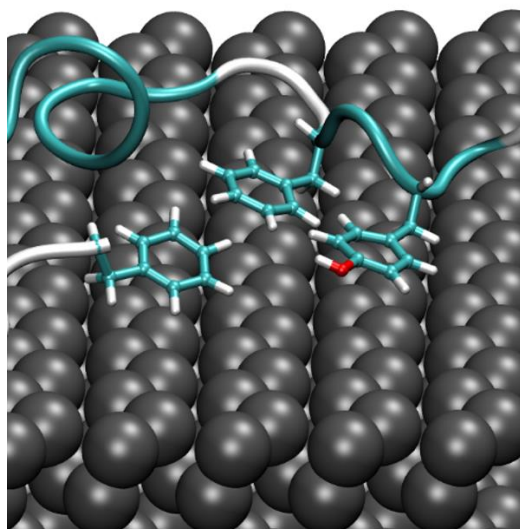
Figure S6. The residues with aromatic structure (B24-B26) act with BPQDs surface. Related to Figure

4.
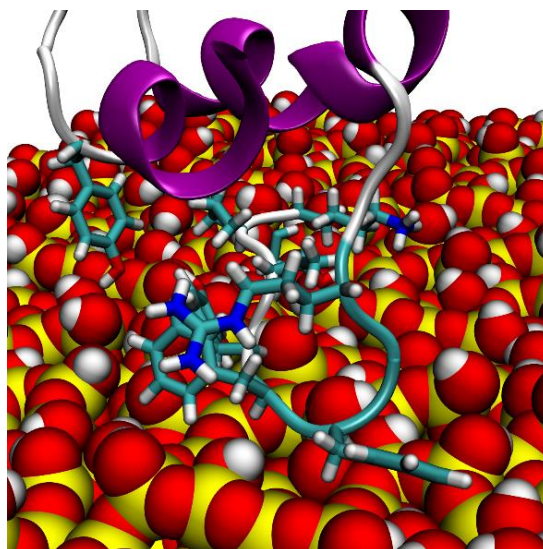
Figure S7. The snapshot of the interaction between insulin and SiNPs surface. Related to Figure 4.
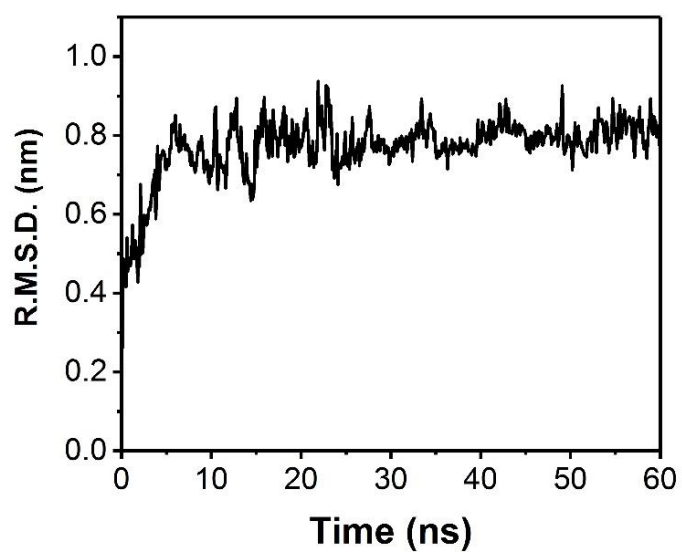
Figure S8. The R.M.S.D. varying with time of insulin with SiNPs. Related to Figure 4.

TRANSPARENT METHODS

Materials. Bovine insulin (>99%) was purchased from Absin Bioscience, Inc. (Shanghai, China). Bulk BP (99.998%) was purchased from Nanjing XFNANO Materials Tech Co., Ltd. (Nanjing, China). N-Methyl-2-pyrrolidinone (NMP, 99.5%) was obtained from Shanghai Macklin Biochemical Co., Ltd. (Shanghai, China). Thioflavin T (ThT), sodium chloride (NaCl) and acetic acid (HAC) were obtained from Sigma-Aldrich (Shanghai, China). Hydrochloric acid (HCl) and tris(hydroxymethyl)aminomethane (Tris) were obtained from Tianjin Kemiou Chemical Reagent Co., Ltd. (Tianjin, China). Ultrapure water was produced by a Milli-Q water purification system (Millipore Corporation, Billerica, MA).

Synthesis of BPQDs. The BPQDs were prepared by a top-down route using a simple liquid exfoliation technique, as we have previously reported (Xia et al., 2018). First of all, the bulk BP powders were dispersed in NMP evenly via mixing and sonicating for 20 min. Then the mixture was sonicated with an ultrasonic cell disruption system in an ice bath for 6 h at 1000 Hz and 60% power. The ultrasound probe was set to work 2 s with an interval of 4 s. The dispersion was centrifuged for 60 min by gradient centrifugation, and the supernatant at 7000 rpm containing the BPQDs was obtained. Subsequently, the NMP solvent was removed by rotary evaporator and washed 3 times with ultrapure water. The obtained BPQDs resuspended in an aqueous solution were stored at low temperature in the dark.

Insulin Fibrillation in the presence of BPQDs. Bovine insulin was dissolved in 20% v/v glacial acetic acid (HAC) with 25 mM sodium chloride (NaCl) to shorten the incubation time. After mixing for 30 s through a vortex mixer and then fully dissolving in the refrigerator for 10 min, several different concentrations of BPQDs (50, 100, 200, 500 ng/mL) were added. The final concentration of insulin is 2 mg/mL. Finally, the insulin solution with BPQDs were incubated in a constant-temperature oscillating water bath (SW-22, JULABO, at 20 rpm, 60 °C) for one week and aliquots of samples were taken at appropriate intervals.

In order to investigate the possible inhibiting effects of BPQDs on insulin amyloid fibrillation process, 500 ng/mL BPQDs were added after 0, 10, 24, 35, 48 h of insulin incubation, respectively. The incubation conditions were the same as above and aliquots of samples were taken at appropriate intervals.

For depolymerization assay, we investigated the effects of BPQDs on insulin mature fibers. After 4 days of insulin incubation, 500 ng/mL BPQDs were added. The incubation conditions were the same as above and aliquots of samples were taken at appropriate intervals.

Thioflavin-T fluorescence assays. A droplet of 10 μL sample was taken and diluted with 2 mL ThT solution (20 μM at pH 7.2, 20 mM Tris-HCl). After static staining for 2 min, the fluorescence intensity of ThT was measured by a fluorescence spectrophotometer (Hitachi) at excitation of 450 nm in a 1 cm quartz cuvette with both excitation and emission slit widths at 5 nm. The fluorescence signal was recorded between 460 and 550 nm, and the emission at 485 nm was used to monitor the kinetics of insulin fibrillation.

Far-UV circular dichroism (CD) spectroscopy. The secondary structure changes of insulin fibrillation process were probed by far-UV CD using a JASCO J-810 spectropolarimeter. After samples were diluted twice with ultrapure water, the spectra were recorded between 190 and 250 nm, with a response time of 1 s and a band width of 2 nm at room temperature using a 0.1 mm optical path length quartz cell. All data were scanned three times and averaged. The secondary structure is analyzed by http://bestsel.elte.hu.

Atomic force microscopy (AFM) characterization. The sample was diluted 50-fold with ultrapure water, and 50 µL of the sample was evenly dropped on freshly cleaved mica. After settling for 1 h, the mica was dried with N_2. Subsequently, the mica was slowly rinsed with ultrapure water to remove salt in AFM images, and finally dried with N_2 again. The AFM (Nanosurf C3000 Controller) was operated in tapping mode in the air using the Tap190-AI-G probe. AFM images were processed using Gwyddion analysis software.

Molecular dynamics simulation. The structure of insulin was obtained from the PDB database (PDB: 5MIZ and PDB:2OMQ for the monomer and the β-sheet fragment, respectively) and prepared at pH 2 (Martinez-Rosell et al., 2017). According to that the native structure is stabilized by three disulfide bridges and they are retained in fibrils, we keep these disulfide bridges in 5MIZ (Hua and Weiss, 2004) Both the N-terminus and C-terminus of 2OMQ were capped to resemble the neural peptide linkage of the insulin. Based on the crystal database (Brown and Rundqvist, 1965), the BPQDs used in the simulation was two layers with a size of 3 nm×3 nm by referring our TEM results. The minimum distance between the protein and the BPQDs was at least 6 angstroms to allow the insulin to freely rotated and adjust its orientation while reducing the diffusion time approaching the BPQDs. The distance between the insulin/BPQDs and the box-boundary was at least 2 nm. The amorphous models and force field parameters of SiNPs surface are developed by Heinz and coworkers (Emami et al., 2014).

We performed MD simulation in amber99sb-ildn force field coupling with TIP3P water model (Jorgensen et al., 1983) since previous MD simulation studies have shown that this kind of combination perform well for the protein system. The interaction potential parameters of the BPQDs was from the ref. (Jiang and Park, 2015) 25mM NaCl were added and these systems are neutral. After energy minimization, we did the production run. The systems were at 60 °C and 2 fs step was made use of integrating the equations of motion. The nonbonded cutoff distance was 12 angstrom and the long-range electrostatics interaction were calculated by using the Particle Mesh Ewald (PME) method (Essmann et al., 1995). The R.M.S.D. is in Figure S2 and Figure S8. Only the last 10 ns of each simulation was used for analysis. The MD simulation results were analyzed using the analysis program in the GROMACS 5.1.4 package and visual molecular dynamics (VMD).

Cell toxicity assays. The cytotoxicity of insulin fibers to PC12 cells was investigated using MTT (3-(4,5-dimethyl-2-thiazolyl)-2,5-diphenyl-2-H-tetrazolium bromide) assay. Firstly, insulin with or without different concentrations of BPQDs incubated for 5 days, and then samples were added to a 96-well cell culture plate with PC12 cells. The final concentration of insulin was 5 µM. After the PC12 cells were further incubated for 24 h, the cells were treated with MTT and formazan was dissolved in

DMSO. Finally, the absorbance values of formazan at 570 nm was measured with a multiskan (Thermo Scientific) to obtain the relative activity of the cells. The experiment was repeated 6 times for each set of samples. All experiments were performed under aseptic conditions.

SUPPLEMENTAL REFERENCES

Brown, A. and Rundqvist, S. (1965). Refinement of crystal structure of black phosphorus. Acta Crystallographica, 19, 684-685.

Emami, F. S., Puddu, V., Berry, R. J., Varshney, V., Patwardhan, S. V., Perry, C. C. and Heinz, H. (2014). Force field and a surface model database for silica to simulate interfacial properties in atomic resolution. Chemistry of Materials, 26, 2647-2658.

Essmann, U., Perera, L., Berkowitz, M. L., Darden, T., Lee, H. and Pedersen, L. G. (1995). A smooth particle mesh Ewald method. The Journal of Chemical Physics, 103, 8577-8593.

Hua, Q. X. and Weiss, M. A. (2004). Mechanism of insulin fibrillation: the structure of insulin under amyloidogenic conditions resembles a protein-folding intermediate. J Biol Chem, 279, 21449-60.

Jiang, J.-W. and Park, H. S. (2015). A Gaussian treatment for the friction issue of Lennard-Jones potential in layered materials: Application to friction between graphene, MoS_2, and black phosphorus. Journal of Applied Physics, 117, 124304.

Jorgensen, W. L., Chandrasekhar, J., Madura, J. D., Impey, R. W. and Klein, M. L. (1983). Comparison of simple potential functions for simulating liquid water. J Chem Phys, 79, 926.

Martinez-Rosell, G., Giorgino, T. and De Fabritiis, G. (2017). PlayMolecule ProteinPrepare: a web application for protein preparation for molecular dynamics simulations. J Chem Inf Model, 57, 1511-1516.

Xia, Y., Wang, S., Huang, R., Su, R., Qi, W. and He, Z. (2018). Adsorption-desorption behavior of black phosphorus quantum dots on mucin surface. Langmuir, 34, 8508-8515.